Supplementary Information for

Method to extract multiple states in F_1-ATPase rotation experiments from jump distributions

Sándor Volkán-Kacsó, Luan Q. Le, Kaicheng Zhu, Haibin Su, Rudolph A. Marcus

Sándor Volkán-Kacsó, Haibin Su and Rudolph A. Marcus.
E-mail: svk@caltech.edu, haibinsu@ust.hk, ram@caltech.edu

This PDF file includes:

Friday 18th October, 2019

1. Methods: analysis of experimental trajectories

A. Dwell and transition selection criteria . The trajectory of interest was provided by H. Ueno and H. Noji and covers most of the experimental time recorded (and stored in file 'Rotation2.txt'), i.e, revolutions 5 – 1765. As can be seen in Fig. S1, angular distribution of the bead shows three distinct peaks. However, they show uneven spacing rather than usual 120° gap, suggesting some factors (e.g. anisotropy in the local environment of the rotary probe due to surface roughness of the microscope slide or F_1-ATPase being in a tilted position due to the unevenness of the microscope slide) affecting the bead rotation.

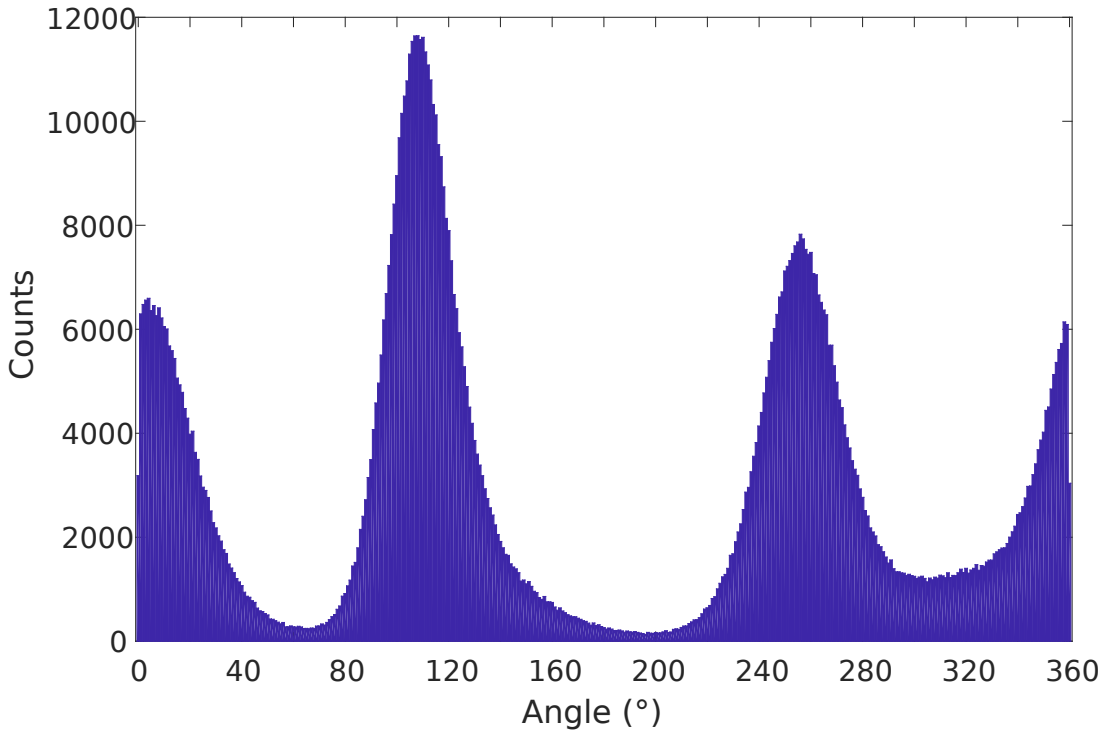

Fig. S1. Distribution of bead positions.

Due to uneven spacing between dwells throughout the trajectory, criteria for selecting dwells into a "high-quality" group were:

1. Transition gaps between dwells should fall within $120^\circ \pm \delta_g$
2. Means of dwells where transitions start should be within $\pm\ \delta_d$ from catalytic dwell values of 0° , 120° and 240°
3. Relatively smooth rather than abrupt and jagged motions of bead during transitions

Examples of such 'high quality' dwells are shown in Fig. S2 by considering $\delta_g = 10^\circ$ and $\delta_d = 5^\circ$. The starting and ending of transitions were selected manually, which will define the ending and starting of dwells respectively. Based on the starting and ending of dwells, the average of dwells could be calculated.

B. Definition of angle and angular jump. Angles used in the analysis were defined as the bead's positions as shown in Fig.S2. The angles were converted to degrees and shifted to fall within 0° – 120°.

The average of dwells where jumps start/end were used as reference angles for starting/ending of transition while mean angular jump of the dwells would be starting/ending angular jump for the transition.

The angular jump was calculated based on the angular difference between angles of two adjacent time frames as follows:

$$\frac{\Delta\theta}{\Delta t}\left(\theta_t\right) = (\theta_{t+1} - \theta_t) \times 360 \times 100\ (^\circ/ms), \qquad [S1]$$

where t is frame t^{th}. The time resolution is 10^5 frames/s.

C. Gaussian fitting of angular jump .

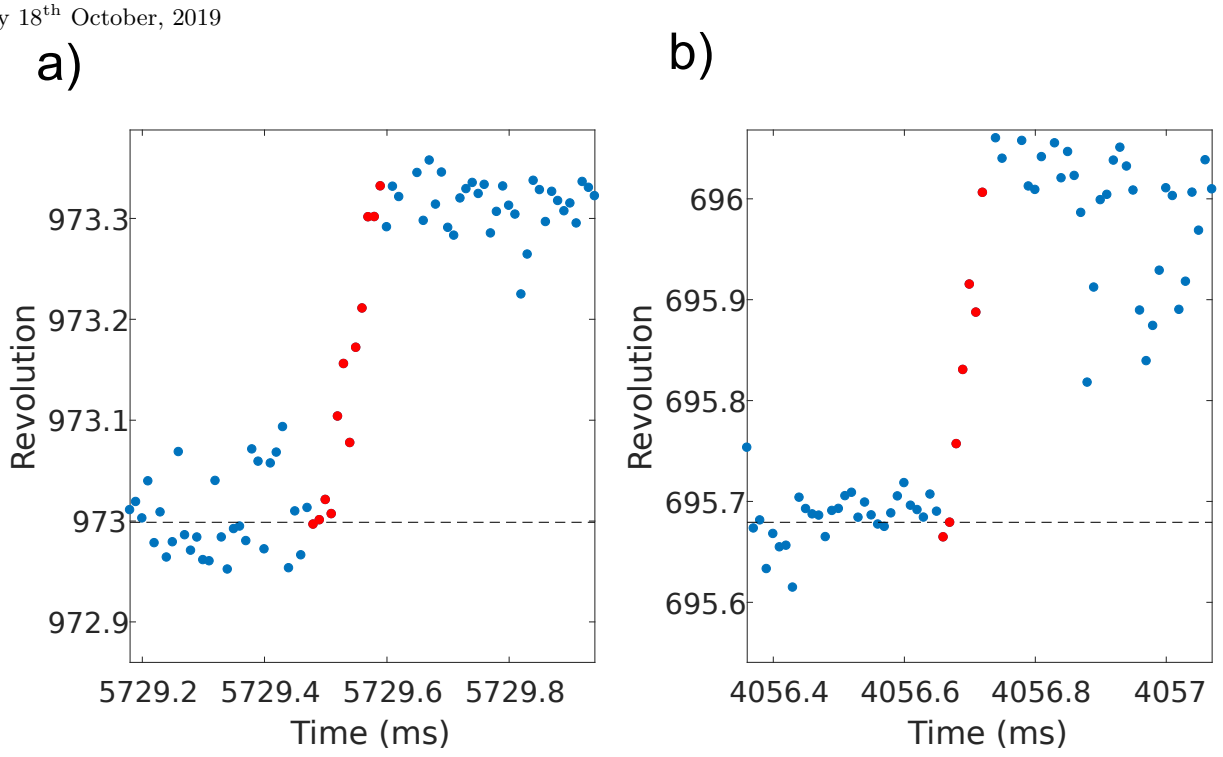

Fig. S2. (a,b) Illustration of transitions selected for analysis based on the aforementioned criteria. Dotted lines indicate mean of dwells. Points belonging to transitions are marked in red.

C.1. Binning of angular jump. The histogram of angular jump was constructed based on the following parameters:

- Angular tolerance ϵ
- Angular step Δ
- Histogram bin size bn
- Angular jump limits $\left(\frac{\Delta\theta}{\Delta t}\right)_{min}$ and $\left(\frac{\Delta\theta}{\Delta t}\right)_{max}$.

C.2. Gaussian fitting form. The Gaussian fitting formula has the following form:

$$P(v) = \begin{cases} \frac{1}{\sqrt{2\pi\sigma^2}} e^{\frac{-(\frac{\Delta\theta}{\Delta t}-\mu)^2}{2\sigma^2}} & \text{for 1 Gaussian} \\ \sum_{i=1}^{2} p_i \frac{1}{\sqrt{2\pi\sigma_i^2}} e^{\frac{-(\frac{\Delta\theta}{\Delta t}-\mu_i)^2}{2\sigma_i^2}} & \text{for 2 Gaussian} \end{cases} \quad [S2]$$

where μ is average angular jump, σ is standard deviation and proportion of Gaussian is p. For double Gaussian, the average angular jump and average standard deviation were calculated as follows:

$$\left\langle \frac{\Delta\theta}{\Delta t} \right\rangle = p_1\mu_1 + p_2\mu_2 \quad [S3]$$

$$\langle\sigma\rangle^2 = p_1^2\sigma_1^2 + p_2^2\sigma_2^2 \quad [S4]$$

C.3. Fitting procedure. For a given angular position θ, the procedure is as follows:

1. Angles within $\theta \pm \epsilon$ were considered as θ.
2. Angular jumps of all selected angles which are within angular jump limits were used to plot histogram with bin size bn.
3. The histogram was then fitted with Gaussian distribution with number of Gaussian is either one or two depending on the angle of interest. The fitting was done via Gaussian mixture model in Matlab.
4. Steps 1 – 3 were repeated for other angles by adding the angular step Δ.

D. Angular jump - Angle distribution. Angular jump - angle distribution was plotted as a two dimensional histogram for a large range of angle covering a majority of 120° transition (e.g 20° - 90°) with bin numbers n_j and n_θ for angular jump and angle respectively (e.g $n_j = 12, n_\theta = 13$). The counts correspond to the number of data points falling within the ranges of angular jumps and angles associated with each bins. For example,a bin at $n_{\theta p}$ and n_{jq} requires: $\theta_p \leq \theta \leq \theta_{p+1}$ and $\left(\frac{\Delta\theta}{\Delta t}\right)_q \leq \frac{\Delta\theta}{\Delta t} \leq \left(\frac{\Delta\theta}{\Delta t}\right)_{q+1}$.

Since there are limited data for smaller range of 40° - 80°, cutoffs for maximum and minimum number of counts are used to increase necessary contrast (e.g counts ≥ 60 were all considered as 60, and ≤ 20 were considered as 20). The angular jump distributions at each angular bins were normalized. The whole distribution was then smoothed by interpolation between bins.

E. Robustness of angular jump - angular position profile.

E.1. Alternative definition of angular position. Besides using the bead's angular positions, the angular difference between the bead and mean of starting dwell could be considered as angular position. This would mean that all transitions start at exactly 0° by shifting all points within a transition with respect to the mean of dwells.

The angular jump distribution shows dependency on how angular positions are defined, as shown in Fig.S5. However, Fig.S3 shows that the overall angular jump - angular position profile is robust and doesn't get affected by different definitions. It is important to note that the shifting may have larger effect when means of dwells vary more than the current limit of variation of 10°. Besides, the data set can be extended by relaxing the third criteria. The parameters used were $\epsilon = 3°$, $\Delta = 3°$, bn = 20, $v_{min} = -\infty, v_{max} = +\infty$ or $v_{min} = -5000°/ms, v_{max} = 6500°/ms$. The starting and ending angles were $-3°$ and 130° respectively.

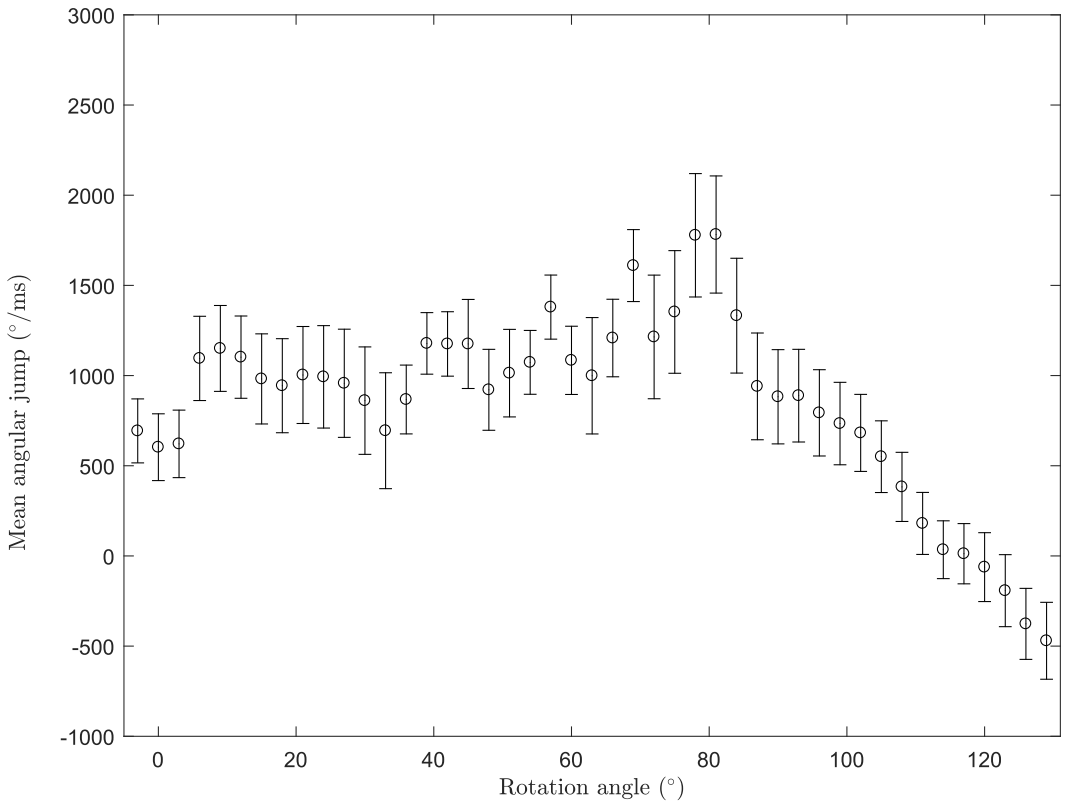

Fig. S3. The average angular jump - angular position profiles subjected to changes in angular jump limits and definition of angular positions. The error bars take into account uncertainty of data selection and finite number of data points.

E.2. Beyond high quality group via transition $0° - 120°$**.** The jump profile of all transitions within $0° - 120°$, shown in Fig. S4, displays an overall similarity with the one obtained from 'high quality' group. However, there are some differences in initial part of 10° lacking the rise of angular jump which is due to the ambiguity of boundary between dwells and starting of transitions. In the latter part of 120°, angular jump drops to zero at around 113°, which may be due to uneven gap when all dwells are taken into account.

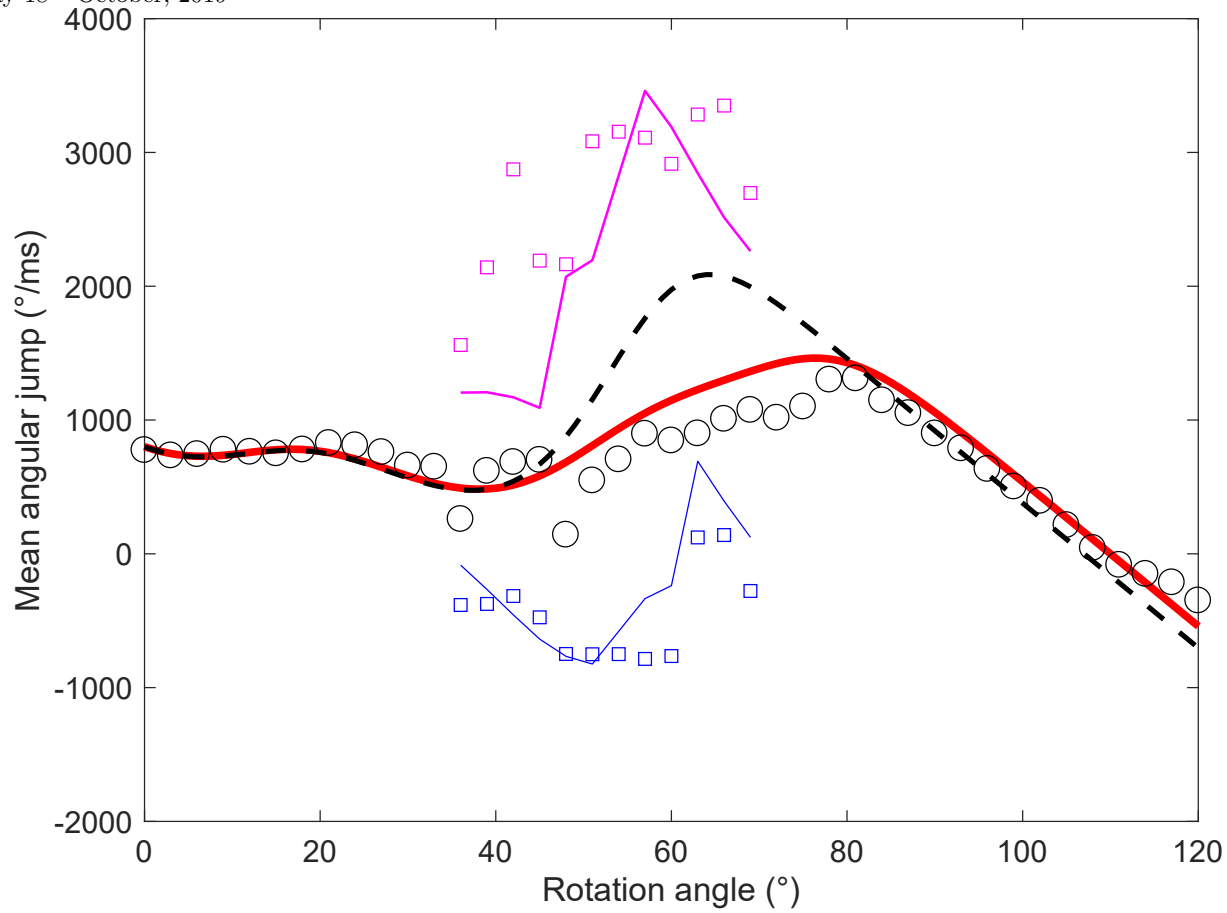

Fig. S4. Average angular jump profile when all transitions of $0^\circ - 120^\circ$ within revolution 5 - 1765 were analyzed.

F. Some limitations in current analysis.

- There are no plausible physical reasonings to accurately define starting and ending point of dwells and transitions, causing the angles within $0^\circ - 10^\circ$ and $110^\circ - 130^\circ$ having high number of small angular jump. The points corresponding to small angular velocities could belong to within dwells, suggesting a feasibility to ignore them for data analysis.

- The existence of double Gaussian is also feasible at other angles outside $40^\circ - 75^\circ$, as shown in Fig.S6. However, limited data hinder high resolution to distinguish close distance between peaks or low proportion of the other peak at other angles.

G. Extraction of rate constants, spring constant, diffusion constant and relaxation time from dwells. Dwell time distribution, as shown in Fig. S7 shows double exponential behavior. The rate constants, the values of two exponents, are 920 s^{-1} and 2000 s^{-1} for hydrolysis and Pi release respectively. Spring constants are extracted from probability distribution of bead positions which is assumed to follow Boltzmann distribution during catalytic dwells. Distributions of spring constants are obtained in Fig. S8 which shows the average value approximately of 55 - 75 pN.nm/rad^2, consistent with previous results.

Relaxation time can be obtained from the bead's angular position correlation during dwells. By assuming harmonic motion under Gaussian white noise, the position correlation is:

$$\langle \theta(t_0 + t)\theta(t_0) \rangle = \frac{k_B T}{k} e^{-\gamma t} \text{ where } \gamma = \frac{D\kappa}{k_B T} \qquad [S5]$$

where k_B,k and D are Boltzmann constant, stiffness of linker and diffusion constant of the bead respectively. Fig. S9 shows position correlation with relaxation time of 14 μs. The diffusion coefficient of the bead is estimated to be approximately 4.1×10^3 rad^2/s given a value of spring constant κ of 72 pN.nm. For a comparison, using a continuum model(1) with ideal spherical bead and neglecting any effects due to the surface, yields a diffusion coefficient estimate of $\sim 1.2 \times 10^3$ rad^2/s (cf. Table S1). This continuum model can be also used to provide an estimate for a rotation diffusion coefficient for a diffusion near the top of a barrier during a transition. Using the bead as a 4 nm analogue for the F_1-ATPase structure, it yields a diffusion coefficient of about $10^7 rad^2/\mu s$ or roughly 10^4 deg^2 $/\mu s$.

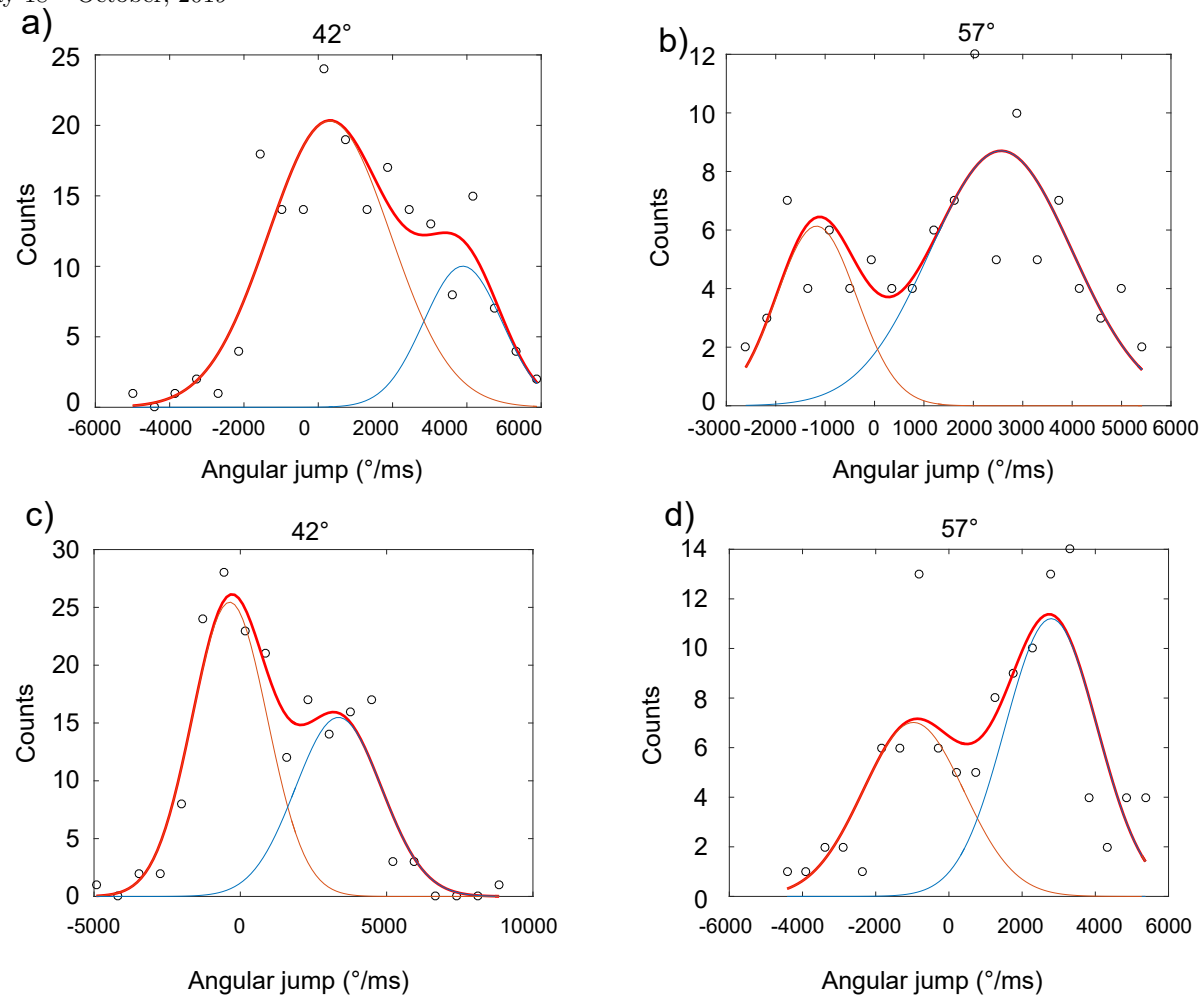

Fig. S5. Changes in angular jump distributions depending on angular positions:(a),(c) based on bead's positions while (b), (d) based on difference between bead's positions and the averages of starting dwells

Since angles from 100° to 130° belong to catalytic state, it is possible to estimate the bead's diffusion coefficient based on the following relation:

$$\sigma^2 = \frac{D}{\gamma \Delta t^2}(1 - e^{-2\gamma \Delta t}) \text{ where } \gamma = \frac{D\kappa}{k_B T} \quad [S6]$$

Based on Fig. S10, with an 'average' σ of 1200 $^\circ/ms$ and relaxation time of 14 μs, a diffusion coefficient estimate of around 4×10^3 rad^2/s results, which is consistent with the value estimated in the previous paragraph from the relaxation time and spring constant in the dwell.

2. Methods: theory and numerical solution the coupled F-P equations

A. Nucleotide transfer model for a torque-generating substep. As previously(2, 3) we assume a "power-stroke" idea in which a reaction in a β subunit is associated with a conformational change that is mechanically coupled to the rotor. The reaction effectively drives the conformational change and the angular displacement from an initial to a final dwell. It could be described as a transfer of nucleotides (ATP or ADP), inorganic phosphate (Pi) or a group of atoms in the protein itself (e.g., a residue, such as Arg.). We also assume that the mechanical coupling is elastic.

We assume that the fluctuations of the reaction coordinate q for the molecular transfer process are much faster than the fluctuations of the rotor angle θ monitored by the probe attached to the γ shaft. The timescale of the fast coordinate q are tens of nanoseconds or faster, while that of θ is microseconds or slower. At the same time, the free energy profile $G_0(q)$ of the transfer is bistable with a large barrier resulting in rare transition events, with rates of 10^3 s^{-1} or slower. In other words, transitions are rare but fast, therefore a quasi-static θ can be assumed during any particular transition. Hence forward and reverse rate constants are given as $k_f(\theta)$ and $k_b(\theta)$. These rate constants have been calculated using transition state ideas and assuming that the coupling between the γ rotor angle θ and the reaction coordinate in the β subunit q is elastic with an effective spring constant of $\kappa_{\gamma\beta}$. The rate constants were shown to follow an exponential dependence on θ over a range of

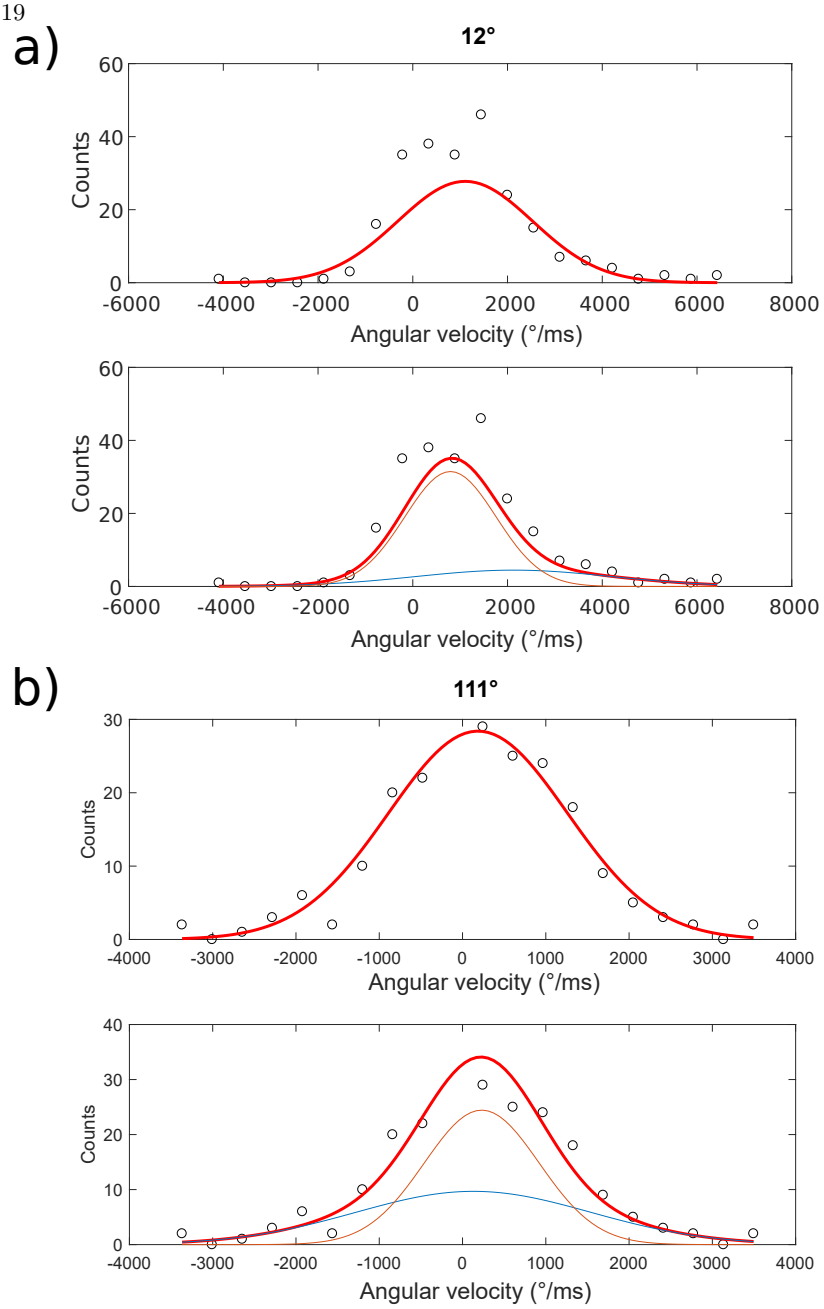

Fig. S6. Comparison for single and double Gaussian fitting of angular jump distribution at (a) 12° and (b) 111°

angles probed in single-molecule stalling and controlled rotation experiments,

$$k_f(\theta) = k_{f,0} \exp[\beta\alpha_0\kappa_R(\theta_p - \theta_r)(\theta - \theta_0)], \quad [S7]$$

$$k_b(\theta) = k_{b,0} \exp[-\beta(1-\alpha_0)\kappa_R(\theta_p - \theta_r)(\theta - \theta_0)], \quad [S8]$$

where $k_{f,0}$ $k_{b,0}$ are the rate constants at θ_0. Before the fast transition the system fluctuated in the neighborhood of the reactant minimum q_r that corresponds to a dwell angle θ_r; after the transition the system relaxes and fluctuates in the neighborhood of the product minimum q_p that corresponds to another dwell angle θ_p. The dwells are monitored in single molecule imaging experiments which can detect the stepping rotation with step size $(\theta_p - \theta_r)$. It is formally advantageous to chose $\theta_0 = (\theta_p + \theta_r)/2$, resulting in a symmetrical form for the rate constants in Eqs. (S7) and (S8).(4) The quantity α_0 the Brønsted slope,(5–7) which in the assumptions in Eqs. S7 and S8 is a constant,

$$\alpha_0 = \frac{d\ln k_f}{d\ln K} = \frac{\partial \ln k_f/\partial\theta}{\partial \ln(k_f/k_b)/\partial\theta} = 1/2 + \Delta G_0^0/(4\lambda). \quad [S9]$$

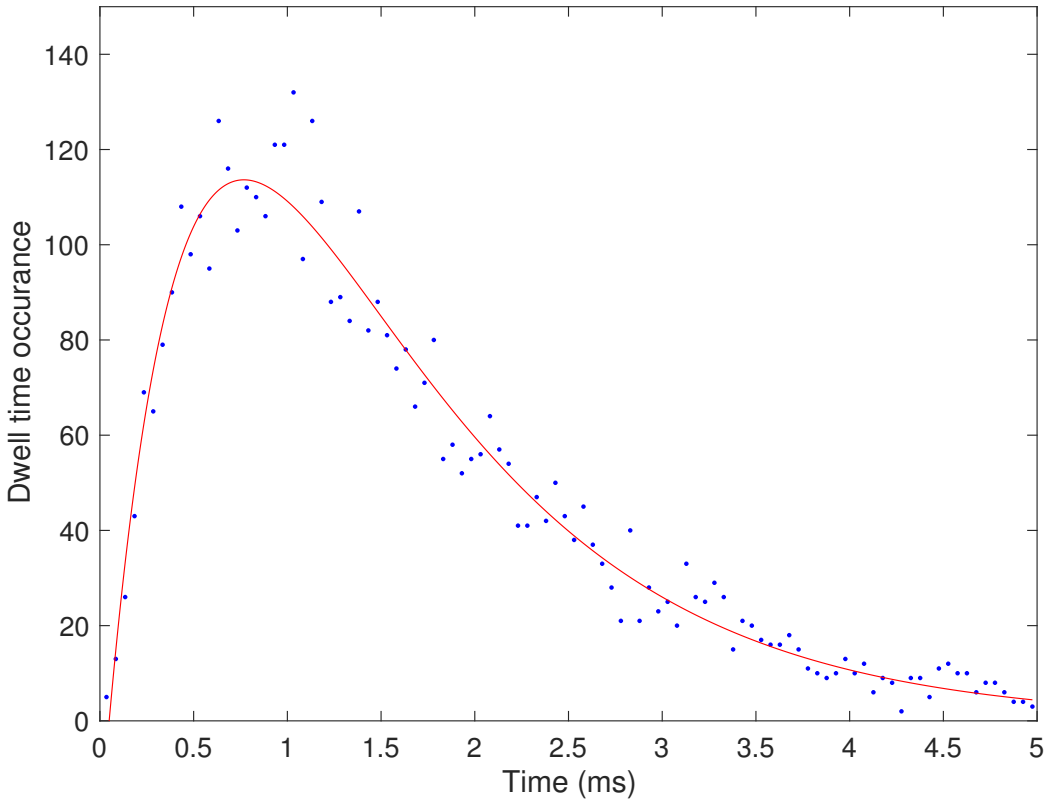

Fig. S7. Dwell time distribution with fitting equation $421e^{-0.92t} - 445e^{-2.01t}$.

B. The Fokker-Planck equations for hydrolysis, Pi release and ATP binding. We assume a transition that follows the catalytic dwell – the rate limiting step at mM ATP concentration – and lasts for 120° until the next catalytic dwell is reached. We assign $i = 0$ to the pre-catalysis state, $i = 1$ to the post-catalysis state. Until the system is the $i = 0$ state, the θ fluctuations are those of the dwell, so the initial time $t = 0$ is when the system jumps to $i = 1$. Next the system either takes a separate Pi release step, or if the latter is concerted with the ATP hydrolysis, it takes the 80° ATP binding step. So, $i = 2$ is either Pi release or ATP binding. In the first scenario, after Pi release, ATP binding follows leading to $i = 3$. After ATP binding the system arrives to the next catalytic dwell at 120° . If the back rates are much lower than the forward rates for all i, then the system of equations describing the behavior in the transitions are:

$$\frac{\partial \rho_1}{\partial t} = D\frac{\partial}{\partial \theta}\left[\beta\kappa_r(\theta-\theta_1)\rho_1\right] + D\frac{\partial^2\rho_1}{\partial\theta^2} - k_{f,1}(\theta)\rho_1, \quad [S10]$$

$$\frac{\partial \rho_2}{\partial t} = D\frac{\partial}{\partial \theta}\left[\beta\kappa_r(\theta-\theta_2)\rho_2\right] + D\frac{\partial^2\rho_2}{\partial\theta^2} - k_{f,2}(\theta)\rho_2 + k_{f,1}(\theta)\rho_1, \quad [S11]$$

$$\frac{\partial \rho_2^*}{\partial t} = D^*\frac{\partial}{\partial \theta}\left[\beta\kappa_r(\theta-\theta_2^*)\rho_2^*\right] + D^*\frac{\partial^2\rho_2^*}{\partial\theta^2} - k_{f,2*}(\theta)\rho_2^* + k_{f,2}(\theta)\rho_2, \quad [S12]$$

$$\frac{\partial \rho_3}{\partial t} = D\frac{\partial}{\partial \theta}\left[\beta\kappa_r(\theta-\theta_3)\rho_3\right] + D\frac{\partial^2\rho_3}{\partial\theta^2} + k_{f,2*}(\theta)\rho_2^*. \quad [S13]$$

C. Numerical solution of the system of diffusion-reaction equations for a 3- or 4-state system. For the numerical solution of the coupled diffusion-reaction equations we use the partial differential equation solver *pdepe* in MatLab.(8) A grid of 100 time steps and 200 angular steps provides adequate resolution in the calculations. For the angular jump distributions a grid of 100 points is used. The advantage of the Fokker-Plack approach is that the numerical solution is fast and thus the exploration of parameter space for the 4^{th} state (θ_2^* and $k_{f0,2^*}$) is feasible for the purpose to extract their value from the trajectories based on the "best fitting" jump profile.

Since in the current treatment the slope for the intermediate 3 occupancy state is not established, we have explored the possibility of any value between 0 and 1. The extreme cases (0 and 1) were plotted in Fig. S11.

C.1. Initial conditions. The system appears to have very similar (or identical) dwell angle before and after catalysis ($\theta_3 \approx \theta_1 \approx 0$). Hence that initial state in the transition is assumed to be just before the system switches to the ATP waiting (empty) state (2).

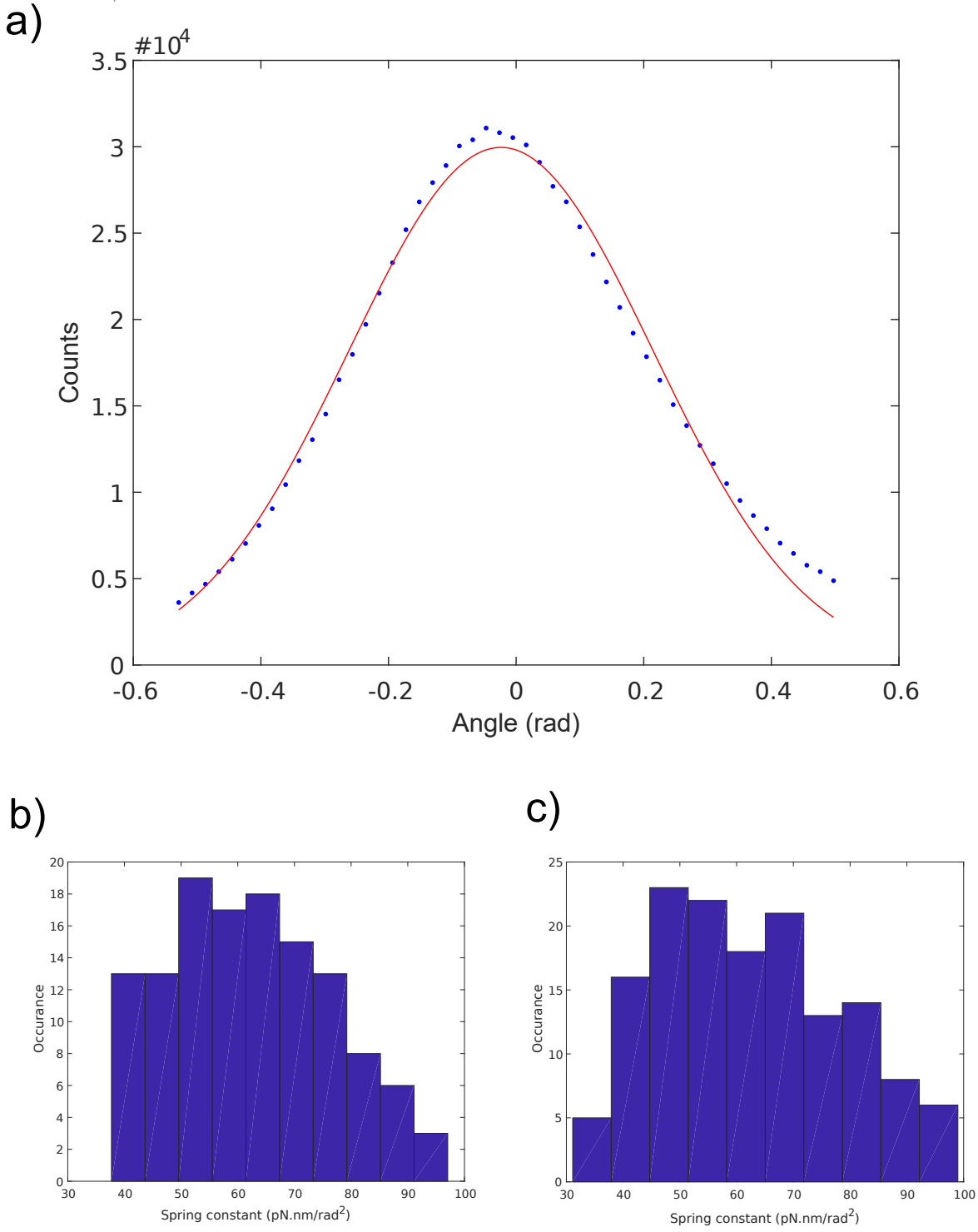

Fig. S8. a) Distribution of the bead's angle from all dwells shows a nice fitting with Gaussian form $3e^{-8.78(\theta+0.02)}$, corresponding to spring constant of 72 $pN.nm/rad^2$. (b-c) Spring constant distributions obtained from starting and ending dwells respectively

We note that in the statistical procedure there is some uncertainty about the state of the system for the first data point in the transition. In the numerical simulations we assumed that the system spends about 1 frame (10μs) in the P_i state (1) before transitioning to the ATP waiting state (2).

Based on the narrow distribution of the initial angle in the transitions produced by the statistical data analysis procedure, a narrow Gaussian distribution of roughly 2° is assumed at $t = 0$.

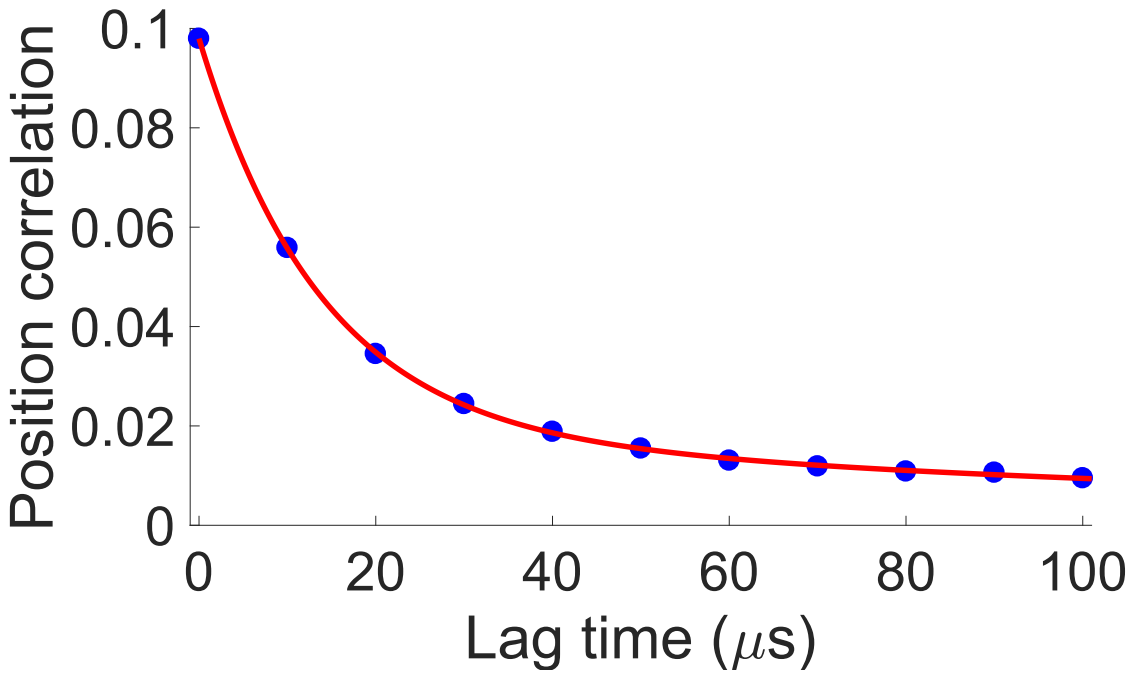

Fig. S9. Bead's angular position correlation obtained from starting dwells. The fitted line is $\langle\theta(t+t_0)\theta(t_0)\rangle = 0.08e^{-t/14} + 0.02e^{-t/140}$. The fast time scale indicates the bead's relaxation time while the slower time scale is due to finite dwell time.

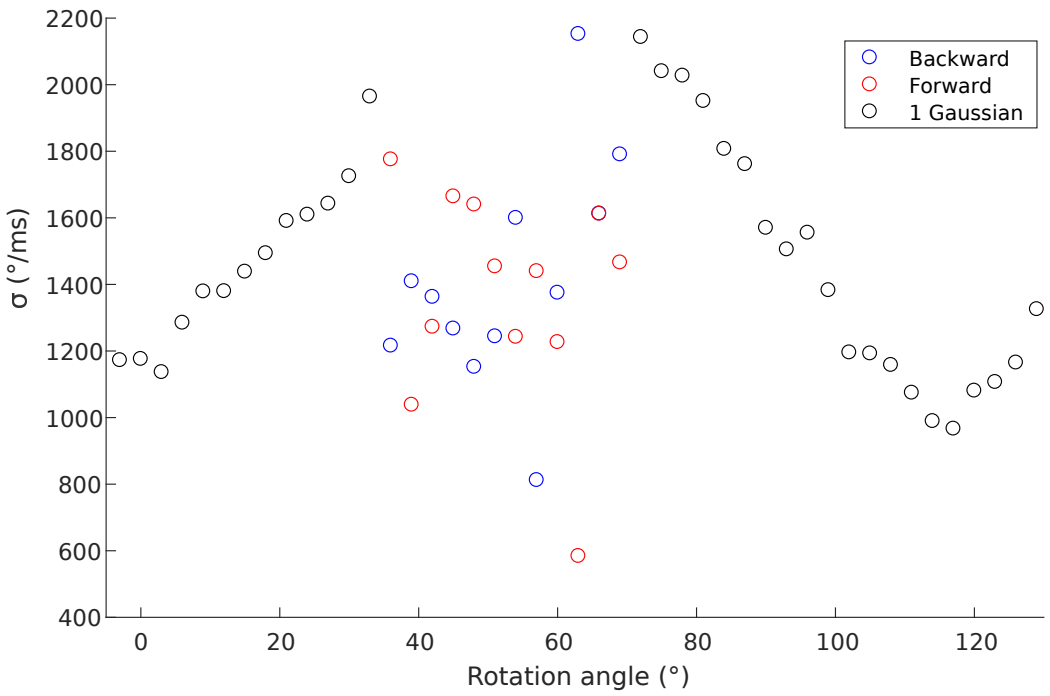

Fig. S10. Width of angular jump distribution at different angles.

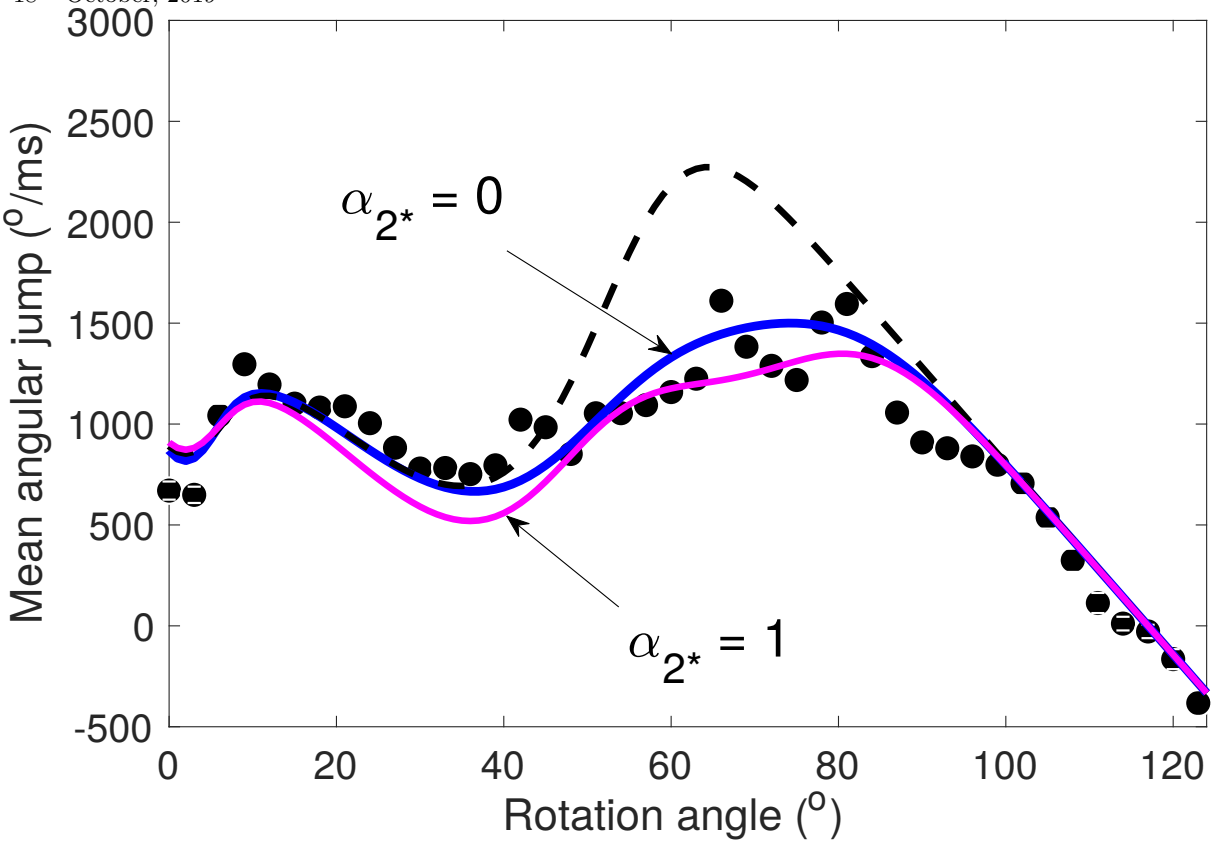

Fig. S11. Mean angular jump profile for of 0 (blue line) and 1 (magenta line) of the metastable state 2^*. A "lifetimes" for the state $1/k_{f2^*}(\theta_{2^*})$ was assumed to be 13 μs and 10 μs, respectively. The 3-state model profile (dashed line) and exponential average jumps (dots) are also plotted for reference.

C.2. Boundary conditions. The angular grid for the solutions stretches 45° beyond the $(0^o, 120^o)$ interval for a transition, to allow for any fluctuations in the dwells. For the 'left' boundary, we assume vanishing probability distributions, $\rho_i(-45^o) = 0$, for all states i. For the 'right' boundary we assume that far enough from the final angle $\theta_3 = 120^o$ the probability flow vanishes for state $i = 3$, $\partial\rho_3/\partial\theta|_{165^o}$. For all non-final states ($i = 1, 2, 2^*$) the right boundary condition is a vanishing probability, $\rho_i(165^o) = 0$.

The boundary conditions should correspond to conditions used in the data analysis, which is necessary when theory and experiment are compared. The right boundary condition assures that the system ends up in state 3, and stays in this state indefinitely. Indeed, during the analysis of data in the transition, the last angular data points in the transitions are always in state 3: once this state is reached, the transition is considered to be complete and no more data will be assigned to that particular transition.

D. Effect of the turnover in the exponential rate constants. .

When a "turnover" occurs at certain θ, the $k(\theta)$ functions reach a maximum, e.g., $k_{f2}(\theta)$ increases with θ then it decreases presumably due to the closing of a cleft in the β subunit.(3) Using a turnover, Eqs. 4 and 5 produced indistinguishable results from those without a turnover (Fig. S11), for the following reason: The width of the fluctuations around the binding dwell θ_2 is $\sim 20°$ (Fig. S9.a), so 50° fluctuations needed to reach the turnover would be very rare even if the system were constrained to state 2. Due to the exponentially increasing $k_{f2}(\theta)$, positive displacements from θ_2 dramatically increase the rate of a transition to the next state, and so the system has reacted before it reaches the "turnover region".

In particular for ATP binding, there may be a turn-over at 100° where ATP binding rate decreases with functional form of $k_{f20}e^{a_2(\pi-\theta-\theta_2)}$. Fig. S12 shows comparable mean angular jump profile with and without considering turn-over for both three and four state model.

E. Reaction sequence and angular jumps..

In the current model, while the system is in some given discrete state i the rotary probe 'feels' elastic torques. The bead fluctuates back and forth about its free energy minimum at the given dwell angle θ_i. A back displacement yields on the average forward (positive) jumps in the experiment while a forward displacement yields mostly backward (negative) jumps. The model state $i = 0$ corresponds to the catalytic dwell before the transitions in the analyzed trajectory (Fig. 1.b). During the kinetic cycle, the system undergoes a progression across states $1 - 2 - 2^* - 3$ (Fig. 3.b), as follows:

1. The Pi-bound state 1 has a dwell at ~ 0, indistinguishable from the catalytic dwell angle. Initially, in the transitions

Table S1. Necessary parameters for description of F_1-ATPase

Parameters	Symbol	Values/Formula
Bead radius	R	20 nm
Radius of rotation for the centroid (from trajectory 1)	r_C	19 nm
Water viscosity	η	10^{-9} pN · s/nm ^{2}
Time step in single-molecule imaging	τ	10 μs
Spring constant for coupling of the rotor angle and single reaction in β	κ_c	16 pN·nm/rad^2
Spring constant for coupling of the rotor with full $\alpha_3\beta_3$ ring	κ_r	72 pN·nm/rad^2
k_BT in pN nm units	k_BT	4.1 pN·nm
Rotational friction coefficient for bead(9)	ζ_B	$8\pi\eta R^3 + 6\pi\eta R r_C^2$
Rate constants versus θ at chemical state $i = \{1...3\}^*$	$k_{f,i}$	$k_{f0,i}\exp[\alpha_i(\theta - \theta_i)]$

* the values are grouped into Table 1 in the main text.

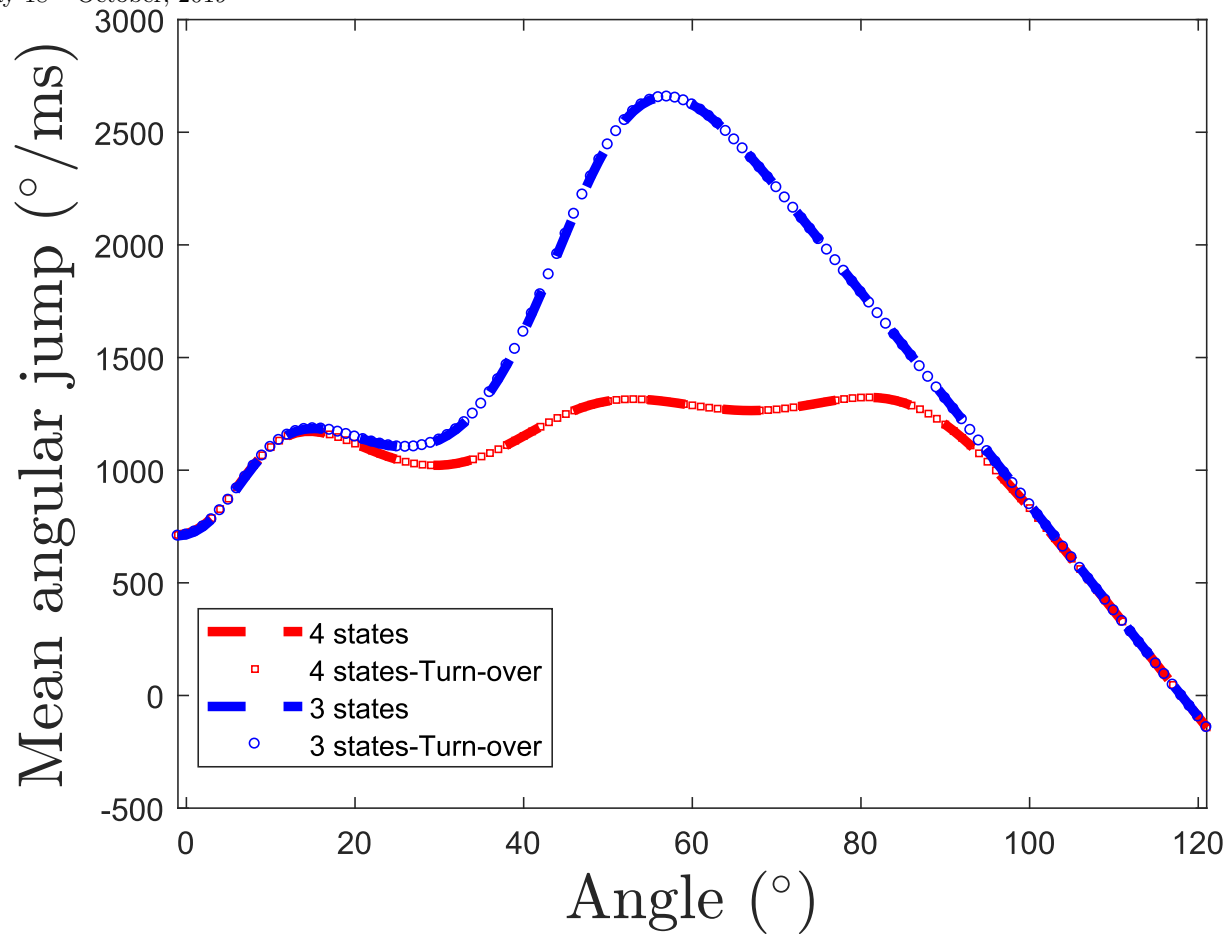

Fig. S12. Mean angular jump profile for three (blue) and four state (red) model with and without turn-over in the ATP binding rate. The turn-over form is assumed to be $k_{f20}e^{a_2(\pi-\theta-\theta_2)}$ for $\theta > \frac{\pi}{2}$.

(Fig. 1.a) we note that in any given trajectory the onset of the ATP waiting empty state occurs within 1/2 Δt, a very small time constant.

2. The system goes into an empty ATP waiting state 2, the bead now starts to relax towards the binding dwell at 40° . Hence at a $\theta < 40°$ there is a positive average jump. The system fluctuates for about 40μs (at 4 mM [ATP]) during which it experiences positive and negative torques. The latter observation explains the appearance of negative average jump profile for lower ATP concentrations highlighted in Fig. S13.b.

3. Next, after ATP binding the system proceeds (within the 4-state model) to a postulated metastable state 2^* and corresponding to an effective dwell at $76^o \pm 5^o$. Between 40° and 76° negative jumps produced in state 2 compete with positive jumps produced in the metastable state. The system is found in the latter 2^* state with a higher probability than in state 2, hence the net positive jumps.

4. ADP release occurs and the system transitions to the final state in this 120° rotation, the pre-catalysis state 3. Its dwell is the catalytic dwell at 120° , so there is initially a large positive torque, detected as a positive branch in the angular jump distribution in Fig. S13.a). The linear θ dependence in the mean angular jump due to visco-elastic relaxation towards the catalytic dwell seen in Fig. 3.a extends beyond 120° : fluctuations of the probe in the hydrolysis state lasting for 1 ms around 120° produces negative torques when it visits $\theta > 120°$ angles.

Mean jump profile at different ATP concentrations and bead size. At increased ATP concentration, a single large peak dominates as seen on Fig. S13.a. The resulting difference between a 3-state model and a 4-state model is more dramatic, than at lower ATP concentrations, and so can be used to further test the consequences of the prediction of an intermediate state 2^*.

When the concentration of ATP is lowered (e.g., to [ATP]=0.4mM), the lifetime of the empty state increases, resulting in a net decrease of the average frequency of an angular jump in a time Δt. A negative mean jump profile in an angular window seen in Fig. S13.b indicates that the fluctuations in a dwell, and so the binding dwell itself, are directly detectable in the trajectories. When the probe is larger, D becomes smaller, resulting in slower rotation seen in Fig. S13.b.

This prediction is consistent with a slower rotation of a 800 degree/ms 'baseline' during transitions using a nanorod (10) twice larger than the bead used in the current analysis.

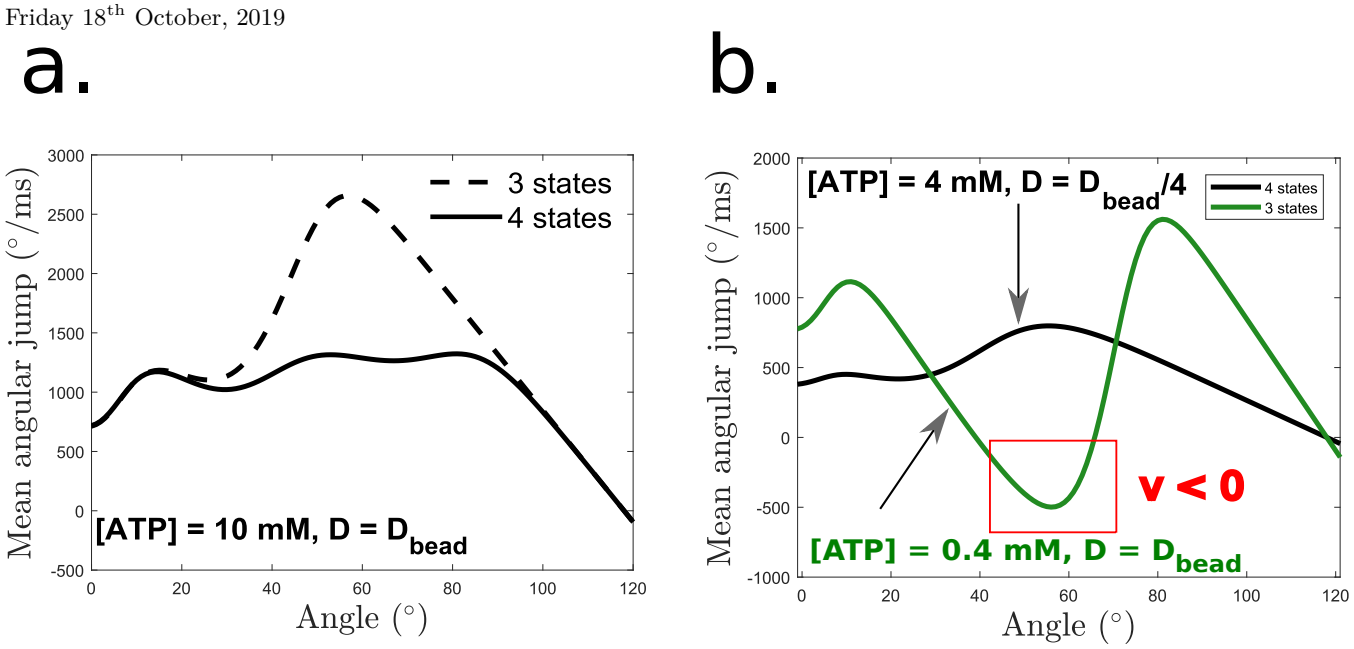

Fig. S13. (a) Theoretical predictions for the angular jump profile at 10 mM ATP concentration for three and four-state model. (b) Theoretical predictions for lower ATP concentration of 0.4 mM (in green) and larger bead, so slower diffusion (black). Negative mean jumps are predicted at lower ATP concentration as the system will spend more time at the binding dwell.

F. Theoretical predictions at different ATP concentrations, bead size and metastable lifetime.

References

1. K Hayashi, H Ueno, R Iino, H Noji, Fluctuation theorem applied to f_1-ATPase. *Phys. Rev. Lett.* **104**, 218103 (2010).
2. S Volkán-Kacsó, RA Marcus, Theory for rates, equilibrium constants, and brønsted slopes in F_1-atpase single molecule imaging experiments. *Proc. Natl. Acad. Sci USA* **112**, 14230–14235 (2015).
3. S Volkán-Kacsó, RA Marcus, Theory of controlled rotation experiments, predictions, tests and comparison with stalling experiments in F_1-atpase. *Proc. Natl. Acad. Sci USA* **113**, 12029–12034 (2016).
4. S Volkán-Kacsó, RA Marcus, Theory of long binding events in single-molecule–controlled rotation experiments on F_1-atpase. *Proc. Natl. Acad. Sci USA* **114**, 7272–7277 (2017).
5. RA Marcus, Theoretical relations among rate constants, barriers, and brønted slopes of chemical reactions. *J. Phys. Chem.* **72**, 891–899 (1968).
6. A Szabo, Kinetics of hemoglobin and transition state theory. *Proc. Natl. Acad. Sci.* **75**, 2108–2111 (1978).
7. T Schweins, A Warshel, Mechanistic analysis of the observed linear free energy relationships in p21ras and related systems. *Biochemistry* **35**, 14232–14243 (1996).
8. , *MATLAB. The language of technical computing (Version R2014b).* (MathWork, Inc., 1984-2014), (2014).
9. R Watanabe, K Hayashi, H Ueno, H Noji, Catalysis-enhancement via rotary fluctuation of f1-ATPase. *Biophys. J.* **105**, 2385 – 2391 (2013).
10. H Sielaff, et al., Power stroke angular velocity profiles of archaeal A-ATP synthase versus thermophilic and mesophilic F-ATP synthase molecular motors. *J. Biol. Chem.* **116**, 745240 (2016).

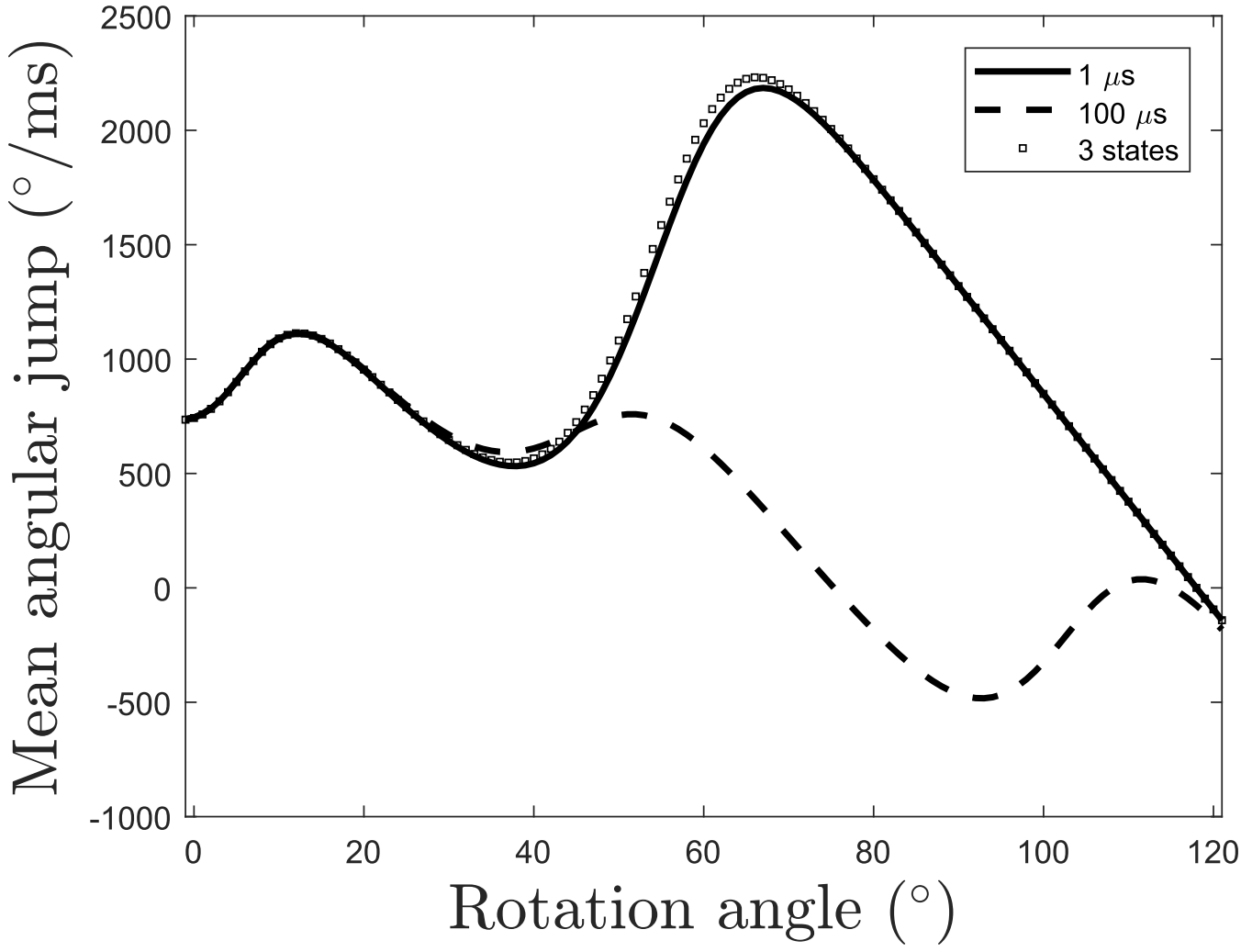

Fig. S14. Angular jump profile for three state (square) and four state. The four state model has different lifetime of metastable state: 1 μs (solid line) and 100 μs (dashed line). Longer lifetime will show another linear slope corresponding to the bead's relaxation time at metastable state.